SI Appendix for

Tissue self-organization based on collective cell migration by contact activation of locomotion and chemotaxis

Taihei Fujimori[1], Akihiko Nakajima[1,2], Nao Shimada[1] and Satoshi Sawai*[1,2]

[1] Graduate School of Arts and Sciences, University of Tokyo, Komaba, Meguro-ku, Tokyo 153-8902, Japan.
[2] Research Center for Complex Systems Biology, University of Tokyo, Komaba, Meguro-ku, Tokyo 153-8902, Japan.

*Correspondence to: cssawai@mail.ecc.u-tokyo.ac.jp

Supplementary Materials and Methods

Plasmid construction. His-tagged TgrB1 and TgrC1 expression vectors pA15-tgrB1^{ext}-His$_6$-2H3term and pA15-tgrC1^{ext}-His$_6$-2H3term were constructed as follows. The expression cassette of pA15-GFP(S/T) was replaced with an expression cassette harboring the *act15* promoter, a *Cla*I/*Xho*I cloning cite and 2H3 terminator by *Xba*I and *Hin*dIII digest (pA15-2H3term). Complementary strands of synthetic His$_6$-tag DNA oligos (Fasmac) were annealed and inserted into the pA15-2H3term vector at *Cla*I/*Xho*I sites by ligation. Genomic DNA fragments from the start codon to the codon just before the predicted transmembrane regions (*tgrB1*; Met1 to Thr802. *tgrC1*; Met1 to Asn851) were PCR amplified using Phusion polymerase (New England Biolab). The cloned fragments were verified by DNA sequencing and inserted into the *Cla*I cite of pA15-2H3term using Infusion HD cloning kit (Z9633N, Takara) according to the manufacture's protocol except that reaction volume was 5 μL containing 1μL premix, and the reaction time was extended to 1 hr. TgrB1-RFP TgrC1-GFP expression vectors were constructed as follows. The *tgrB1* gene including the promoter and the ORF except the stop codon was amplified with an additional N-terminal *Nhe*I site and a C-terminal $(G_4S)_2$ linker sequence(1) and a *Cla*I site by PCR. Vector pHygTm(+) was cut by *Xba*I/*Cla*I to replace the *act15* promoter with the amplified *tgrB1* fragment to obtain pHyg-[tgrB1p]:tgrB1-$(G_4S)_2$-mRFP1. The vector with [tgrC1p]:tgrC1-$(G_4S)_2$-GFP was constructed similarly except that the *tgrC1* was cloned into pA15-GFP(S/T) for G418 resistance. A prestalk GFP marker plasmid pEcmAO-GFP was constructed by replacing mRFPmars in pEcmAO-mRFPmars with GFP(S65T) at *Bgl*II and *Xho*I sites.

Transformation. Purified plasmids were used to transform *Dictyostelium* cells by electroporation following a standard protocol(2) and selected using 10 μg/mL G418 or 60 μg/mL Hygromycin. Following strains of *Dictyostelium discoideum* were used for live-cell imaging analysis: AX4 and its derivatives GFP-Lifeact(3)/AX4, Lifeact-mRFPmars(4)/AX4, GFP/*tgrB1*$^-$, tdTomato/*tgrC1*$^-$, GFP-Arp2(5)/AX4, GFP-Myo(6)/PHcrac-RFP/AX4, HSPC300-GFP(7)/Lifeact-mRFPmars/AX4, PakBCRIB-mRFP(7)/GFP-Lifeact/AX4, GFP-Lifeact/mRFPmars-Raf1RBD(8)/AX4, GFP-Lifeact/PHcrac-RFP/AX4, pEcmAO-

GFP/pD19-RFP/AX4, Epac1-camps(9)/AX4, [tgrB1p]:tgrB1-RFP/*tgrB1*$^{-}$, [tgrC1p]:tgrC1-GFP/*tgrC1*$^{-}$, [act15p]:tgrB1-RFP/AX4, [act15p]:tgrC1-GFP/AX4, GFP-Arp2/pD19-RFP/AX4, GFP-Myo/pD19-RFP/AX4. To obtain pEcmAO-GFP/pD19-RFP/AX4, AX4 cells were co-transformed by electroporation with plasmids pEcmAO-GFP and pD19-RFP. Phenotypes of TgrC1 or TgrB1 expressing clones in the respective knockout background varied on a bacteria plate likely due to stringency on the expression level. Clones whose null-phenotype of fruiting bodies were rescued were chosen for analysis.

Cell preparation. Cells were grown in modified HL5 medium(10) with appropriate selection drugs at 22°C using a rotary shaker. To obtain the "streaming-stage" cells, cells were removed of nutrient by 3 repeated cycles of centrifugation at 700 ×*g* for 3 min and resuspension in Phosphate Buffer (PB: 12 mM KH_2PO_4, 8 mM Na_2HPO_4, pH 6.5). Washed cells were suspended at the final density of 5×10^6 cells/mL and shaken for 6 to 8 hr at 125 rpm at 22°C. cAMP pulses (final conc. 50 nM) were applied at 6 min intervals after 1 hr using a peristaltic pump (Masterflex L/S, Cole-Permer).

To obtain "slug-stage" cells, washed cells were suspended in Developmental Buffer (DB: 6 mM KH_2PO_4, 4 mM Na_2HPO_4, 2 mM $MgSO_4$, 0.2 mM $CaCl_2$, pH 6.5) and plated on an agar dish (1% agar (Bacto) in DB) at final density of 6.6×10^3 cells/mm^2 to obtain a monolayer(11). The cells were incubated in a dark condition at 22°C for 17 to 21 hr before collection. Slugs were suspended in 1 mL of PB and mechanically dissociated by running it through a 23G needle (NN-2332R, Termo) back and forth using a syringe 10 times. Dissociated cells were washed and resuspended in 1mL of PB.

Microfabrication. Poly-dimethylsiloxane (PDMS) chambers were fabricated as described previously(12). In brief, blank masks (CBL4006Du-AZP, clean surface technology) were UV-irradiated by laser drawing system (DDB-201-TW, Neoark) and chemically etched to create photomasks. Photoresists SU-8 3005 and 3050 (Microchem,) were used to create molds of the chambers. The thickness of SU-8 which determines the height of the microchamber for observation channel was approximately 4-5 μm for the gradient chamber (Fig. S3A and S5A), 4 μm for the low ceiling chamber for multicellular observations (Fig. S12B). The mask was placed on top of a SU-8 coated wafer and UV-irradiated using a mask aligner (MA-20, Mikasa). The cured SU-8 was used as a mold to fabricate PDMS. Glass cover slips (No. 1 or 1S, 24 × 60 mm or 50 × 60 mm, Matsunami) were washed in four steps using basic detergent, ethanol, NaOH solution, then rinsed in milli-Q water. Washed cover slips were dried at 140°C in a sterilization oven. The cover slips and fabricated PDMS were treated with air plasma, bonded and heated at 75°C for 1 hr.

Flow in microchambers was controlled using a pressure regulator (Microfluidic Flow Control System (MFCS), Fluigent) or a syringe pump (70-4506, Harvard) as described previously(13). A PDMS chamber was connected to the MFCS device with ethylene tetrafluoroethylene (ETFE) tubes. Gradient was reversed by programmed flow control using a MFCS scripting module. In the experiments where purified proteins were perfused (Fig. S10), pipet tips filled with cAMP solution and PB were inserted to chamber inlets and the resulting flow by hydrostatic pressure was used.

Microscopy and Image Analysis. All fluorescence images were obtained by confocal microscopy. With some exceptions (see below), data were obtained by an inverted microscope (Ti-E, Nikon) equipped with a laser confocal point-scanning unit (A1R, Nikon) using a Galvano scanner except for data in Fig. S6A where a fast resonant scanner was employed. For UV-irradiation, 405 nm laser (100 mW CUBE, Coherent, at max power) was employed. For photobleaching of GFP-Arp2 (Fig. 2F-H), 488 nm laser (100 mW CUBE, Coherent, at max power) was used to irradiate 0.25 × 4.88 μm (8 × 157 pixels) rectangular ROI positioned halfway between the ends of F-actin filaments. The length of actin filaments 1.26 sec and 3.15 sec after bleaching were measured manually, and the difference between them was defined as nucleation speed. The displacement of the tip of filament at the same time frames was defined as protrusion speed. Slip speed was calculated by subtracting protrusion speed from nucleation speed.

For data in Fig. 3E, 4F-G, an inverted microscope IX81 (Olympus) equipped with a multi-scan laser confocal unit CSU-X1 (Yokogawa) with EMCCD camera (Evolve512, Photometrics) was used. For data in Fig. 1C-I, 3D, 3F, and Fig. S1A-B, S1G, S8A, S9C-D, S11B-C, S12E, S14A-C, S15A-B an inverted microscope IX83 (Olympus) equipped with CSU-W1 with a EMCCD camera (iXon 888, Andor) was used. 445 nm, 488 nm and 561 nm lasers were used for excitation, and fluorescence images were obtained by appropriate filters. Piezo z-stages were used for z-sectional imaging. Live-cell imaging was performed at 22°C. All images were stored as TIFF files and analyzed using homemade programs in ImageJ and MATLAB (Mathworks).

To obtain relative changes in the cytosolic cAMP level (Fig. 1D,F,H), the ratio of fluorescence intensities of Epac1-camps/AX4 in the CFP-channel ($I_{472/30}$) and the YFP-channel ($I_{542/27}$) was averaged in a rectangle region (24 × 36 pixels). For calculation of the phase by time-delay embedding (Fig. 1E,G,I), the mean fluorescence intensities in the CFP-channel and the YFP-channel images were averaged by moving timeframes (5 time points; 60 sec) and the background was subtracted. The background was obtained by averaging over 31 time points (450 sec) in moving time frames. The average fluorescence intensities $\overline{I(t)}$ were obtained for all positions by 5 × 5 pixels binning. Phase was defined by an angle in the embedding space ($\overline{I(t)}$, $\overline{I(t+75sec)}$). Lifeact-RFP expressing cells were manually tracked during ±3 minutes at each time points.

For quantification in Figure 2E, timelapse series were acquired with 20× objective lens from total of 27 channels. Cells positioned between 95 to 378 μm from the edge of observation channels (473 μm edge-to-edge) were analyzed. Cells were counted as performing 'Chemotaxis' to gradient reversal if the cells formed a contact-free leading edge and migrated toward a new gradient (Fig. 2E). Cell speed in Figures 4A and B was calculated from cell trajectories obtained by manual tracking of cell centroids using the ImageJ MTrackJ plugin.

Quantification of cell morphology (Fig. S4, Fig. S7C-D), was performed as previously described(12) with some extensions. Velocity was obtained by calculating displacement projected normal to the cell contour per unit time and averaged over 3 neighboring positions and 3 time points. The sign of velocity was negative

for inward projections. Localization of Lifeact-RFP or GFP-Lifeact at cell boundaries were calculated by taking the average fluorescence intensities for each 3 × 3 pixels regions at the boundary (rounded coordinates; 500 positions) and dividing it by the mean fluorescence intensities of the cytosolic region for normalization.

Duration of F-actin enrichment at the cell-cell interface (Fig. 3A,B, Fig. S9A,B) was measured based on the appearance of strong F-actin accumulation especially near the periphery of cell-cell contact. For the statistics of cell-cell contact, cells in contact for longer than 2 minutes were counted. For the analysis of head-to-tail pairing in binary cell mixtures (Fig. 3C), relative positioning of cell-types within cell trains were identified and counted manually based on the fluorescent labels. Frequency of pairing was corrected by total detected cell number of each mixed strain to eliminate the cell number bias. Cells attached to vegetative cells or a microsphere (Fig. 3D, Fig. 4D, Fig. S11A) was identified as polarized if the elongated shape at the cell-cell or cell-bead contact region lasted for more than 10 minutes. Protrusive structures from the lateral side of polarized cells that lasted at least 18 sec were counted as lateral pseudopods (Fig. 4E). Cells were counted as showing a 'Response' to cAMP in Fig. 4G if a protrusion toward the cAMP source appeared while a contact-dependent protrusion was lost at the same time.

Observations of regenerating mounds. To obtain a thin agar film, 200 μL of 1% Agar / DB was poured on a glass bottom dish, covered the glass (15 mm diameter) entirely, then removed to leave small residues typically of 30 μm height. 1×10^6 mechanically dissociated cells were pelleted by centrifugation, then resuspended in 10 μL of PB or 1 unit/mL PDE or 1 mg/mL TgrB1 or 1% BSA. Cells were spread on a thin agar film using a pipette tip with care not to touch the agar, and allowed to settle for 10 minutes. A wet Kimwipe was included in the glass bottom dish, and the lid was closed during observation to avoid sample from drying.

Reagents. 100 mM cAMP-Na (A6885, Sigma) solution was dissolved in water and stored at −20°C as a master stock; working solution was 100 μM. Folate (060-01802, Wako) was dissolved in PB at 10 μM and used as a working solution. Fluorescein (231-00092, Wako) was dissolved in water at 1 mM and stored at 4°C. ATTO425 (AD425-21, ATTO TEC) and Alexa594 (A10438, Invitrogen) were dissolved in DMSO at 1 mg/mL and stored at –20°C. SQ22536 (505-44021, Wako) was dissolved in PB at 10 mM and stored at –20°C. Wheat germ agglutinin (WGA: 126-02811, Wako) was dissolved in water at 1 mg/mL and stored at –20°C. cAMP-specific phosphodiesterase (P0520-1UN, SIGMA) was dissolved in PB at 1 to 2 unit/mL and stored at 4°C. Arp2/3 inhibitor CK-666 (SML0006-5MG, SIGMA) was dissolved in DMSO at 100 mM and stored at –20°C. A F-actin inhibitor Latranculin A (125-04363, Wako) was dissolved at 1 mM and stored at –20°C. For micro chamber experiments, 5 μg/mL ATTO425, 3 μM fluorescein or 4 μg/mL Alexa594 was included in the cAMP solution to visualize the gradient profile. For assays of streaming-stage cells in the gradient chamber, 50 μM SQ22536(11, 14) was included in the perfusion to inhibit adenylyl cyclase.

Stimulus delivery by glass needle. A glass needle (Femtotip, Eppendorf) was backloaded with either 100 μM cAMP or 10 μM folate solution in PB containing 10 μM fluorescein (Fig. 3E, Fig. 4F,G). To stimulate cells attached to a coated-microsphere, the needle was positioned approximately 20 μm from the cell of interest using a manipulator (TransferMan, Eppendorf), and cAMP gradient was formed by pressuring the needle at 80 hPa using an injection pump (Femtojet, Eppendorf)(15).

Protein purification. To verify secretion of recombinant proteins, TgrB1^{ext} and TgrC1^{ext} were extracted from growth medium by His Mag Sepharose excel (17-3712-21, GE Healthcare) according to the manufacturer's protocol. The expected 150 kDa band was confirmed by SDS-PAGE and western blot using a 6xHis monoclonal antibody (D291-3, MBL) (Fig. S1D). For lab-scale production, the cells were grown shaken in 660 mL modified HL5 medium for 2 days until they reached approximately 1×10^7 cells/mL. The typical working volume was 660 mL split into two 1 L flasks. The medium was separated from the cells by centrifugation and passed through a syringe filter (0.22 μm or 0.45 μm). The His-tagged protein TgrB1^{ext}-His_6 or TgrC1^{ext}-His_6 was purified by affinity chromatography (AKTA pure 25M2, GE Healthcare) using a nickel-nitrilotriacetic acid (Ni^{2+}-NTA) column (His Trap FF crude 5mL, GE Healthcare). Captured His-tagged protein was eluted in 20 mL of PBS with an optimized concentration of imidazole. 20 mL of the eluate was concentrated 10-fold using a spin column (Amicon Ultra 15mL 50K, Millipore), diluted in 15 mL of PB. The sample was further concentrated to 700 μL using the spin column by repeating the process twice. The final yield based on the absorbance at 280 nm was 0.1-0.6 mg/mL for TgrC1 and 1-1.5 mg/mL for TgrB1. Purified samples were stored in 1.5 mL tube at 4°C.

Coating silica beads with purified proteins. Briefly, 2 to 4 mg of dry beads were suspended in immobilization buffer and mixed with either 20 μg of the purified protein, 20 μg wheat germ agglutinin (WGA) or both. The mixture was incubated overnight at room temperature in a plastic tube gently rotated at 30 rpm. Beads were collected by centrifugation, and resuspended in 0.5 mL of PBS. The process was repeated two more times. The beads were then suspended in 400 μL of inactivation buffer in a plastic tube and gently agitated by rotation at 30 rpm for 1 hr. The inactivated beads were collected by centrifugation and suspended in 0.5 mL of PBS. Washing was repeated thrice, before finally suspending the beads in 0.2 mL of PB. The coated beads were stored at 4°C.

RT-qPCR. Cells from the prestalk and prespore regions were manually collected under a dissecting microscope from approximately 50 slugs using a glass needle. Prestalk and prespore regions were determined by eye based on the slug morphology. Collected prestalk and prespore samples were suspended in 100 μL PB and pelleted by centrifugation (1000 *xg*, 4°C, 5 min). Total RNA was extracted by an automated instrument (Maxwell 16 AS2000, Promega) and reaction wells (Maxwell 16 LEV simplyRNA Cells Kit, AS1270, Promega) according to manufacturer's protocol. Final yield was 7.5~13 ng/μl for prestalk cells and 20.9~41.6 ng/μl for prespore cells. cDNA was synthesized by reverse transcriptase (SuperScriptIII, 18080-

051, Invitrogen) using random primers. Quantitative PCR was carried out using a real-time PCR thermal cycler (System 7500, Applied Biosystems) and SYBR green qPCR mix (THUNDERBIRD SYBR qPCR mix, QPS-201, Toyobo) and gene-specific primer sets. Ribosomal *rnlA* (Ig7) transcript was used as a standard to quantify all target transcripts. Each sample was quantified in three independent wells and the average was obtained. Specificity of primer sets was confirmed by a single peak in the melting curve and a single band of each qPCR products in agarose gel (4%) electrophoresis.

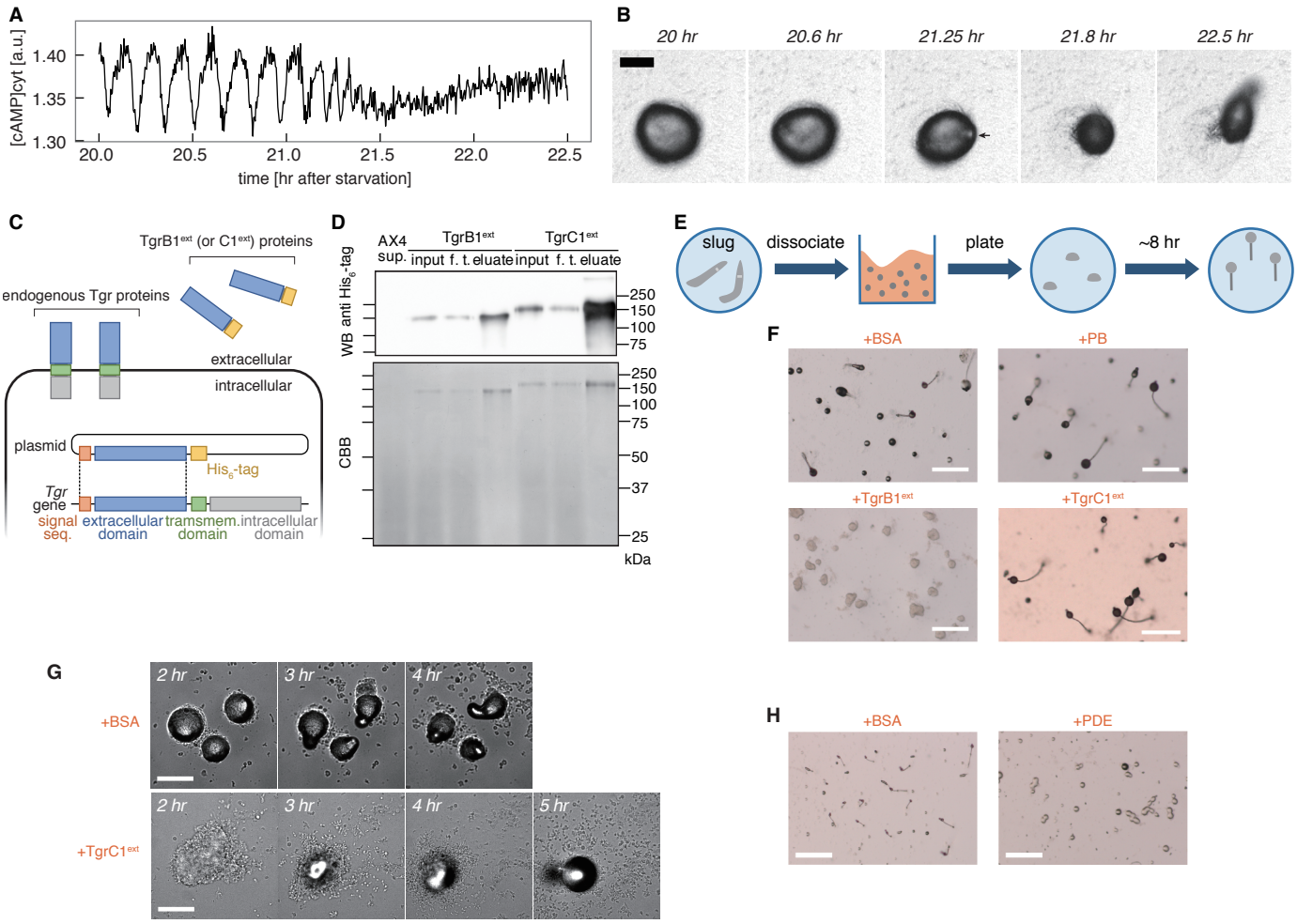

Fig. S1. cAMP oscillations and waves during development. Generation of TgrB1^{ext}, TgrC1^{ext} secreting cells and purification of TgrB1^{ext} and TgrC1^{ext} from extracellular medium. Application of purified TgrB1^{ext} or cAMP-specific phosphodiesterase (PDE) suppresses tip formation.

(**A** and **B**) Timeseries of the mean cytosolic cAMP levels (Epac1-camps/AX4) (A) and bright field images (B) during tip formation. The arrow indicates a mound tip. Scale bar, 200 µm. (**C**) Plasmid construction and protein purification (see Methods for details). (**D**) Coomassie Brilliant Blue (CBB) stained gel after SDS-PAGE (lower panel) and western blotting of the affinity purified TgrB1^{ext} and TgrC1^{ext} from growth media using anti-His$_6$ antibody (upper panel). Lane 1; AX4 supernatant (control), lane 2, 5; input, lane 3, 6; flow through (f. t.), lane 4, 7; eluate. The molecular mass in kDa is indicated. Smears from culture media observed at 25-50 kDa (lanes 2, 5) were eliminated in eluate (lanes 4, 7). (**E**) Experimental scheme of tip formation after dissociation. Slugs developed on a phosphate buffer agar plate were collected and dissociated by passing through a syringe needle. Dissociated cells were allowed to reaggregate on fresh agar and observed 7-8 hr after plating. (**F**) Aggregated cells formed loose mounds without a tip under TgrB1^{ext} application (lower left panel). Fruiting bodies in control conditions (+BSA, +PB) and under TgrC1^{ext} application (upper panels, lower right panels). Scale bars, 500 µm. (**G**) Dispersal and re-aggregation under TgrC1^{ext} application (lower panels; TgrC1^{ext}). Tip formed after 2 hr delay compared to the mock control (upper panels; +BSA). Scale bars, 100 µm. (**H**) Under PDE application, cells formed compacted mounds without a tip (left panel). Fruiting bodies observed in controls (right panel). Scale bars, 500 µm.

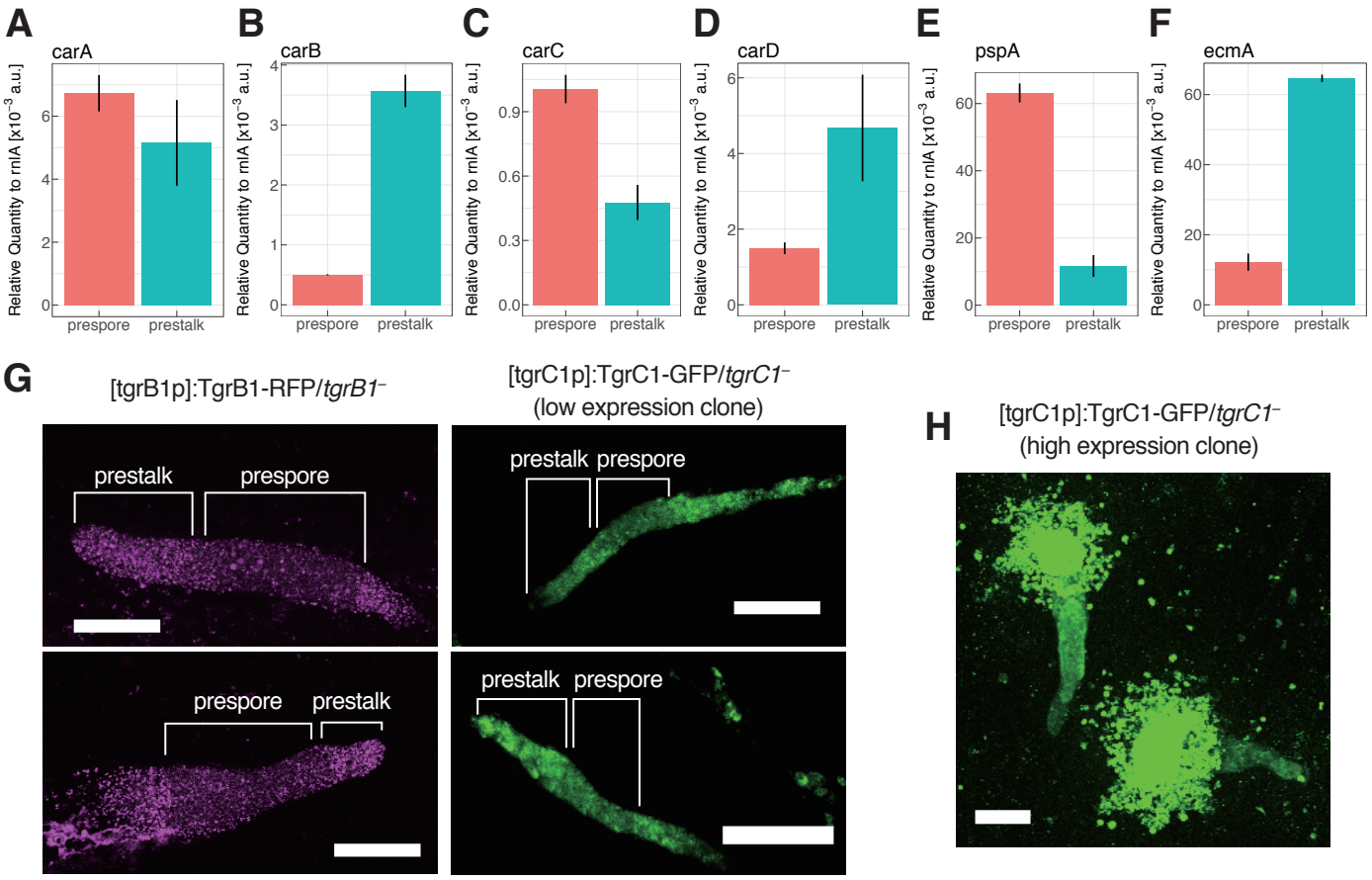

Fig. S2. Differential expression of cAMP receptors and TgrB1/C1.

(**A** to **F**) Slug-stage mRNA quantification of cAMP receptor genes (A-D) and prespore specific *pspA* gene (A) and prestalk-specific *ecmA* gene (F). The expression level was normalized in reference to *rnlA* (see *SI Appendix, Materials and methods*). (**G**) Fluorescent images of slugs expressing [tgrB1p]:TgrB1-RFP in the *tgrB1*$^{-}$ background (left panels) or [tgrC1p]:TgrC1-GFP in *tgrC1*$^{-}$ background (right panels). Developmental defects were rescued in the low expression clones. Scale bar, 100 µm. (**H**) High expression clones of [tgrC1p]:TgrC1-GFP/*tgrC1*$^{-}$ showed failure of many highly fluorescent cells to join the slug after aggregation. Scale bar, 100 µm. Representative clones are shown.

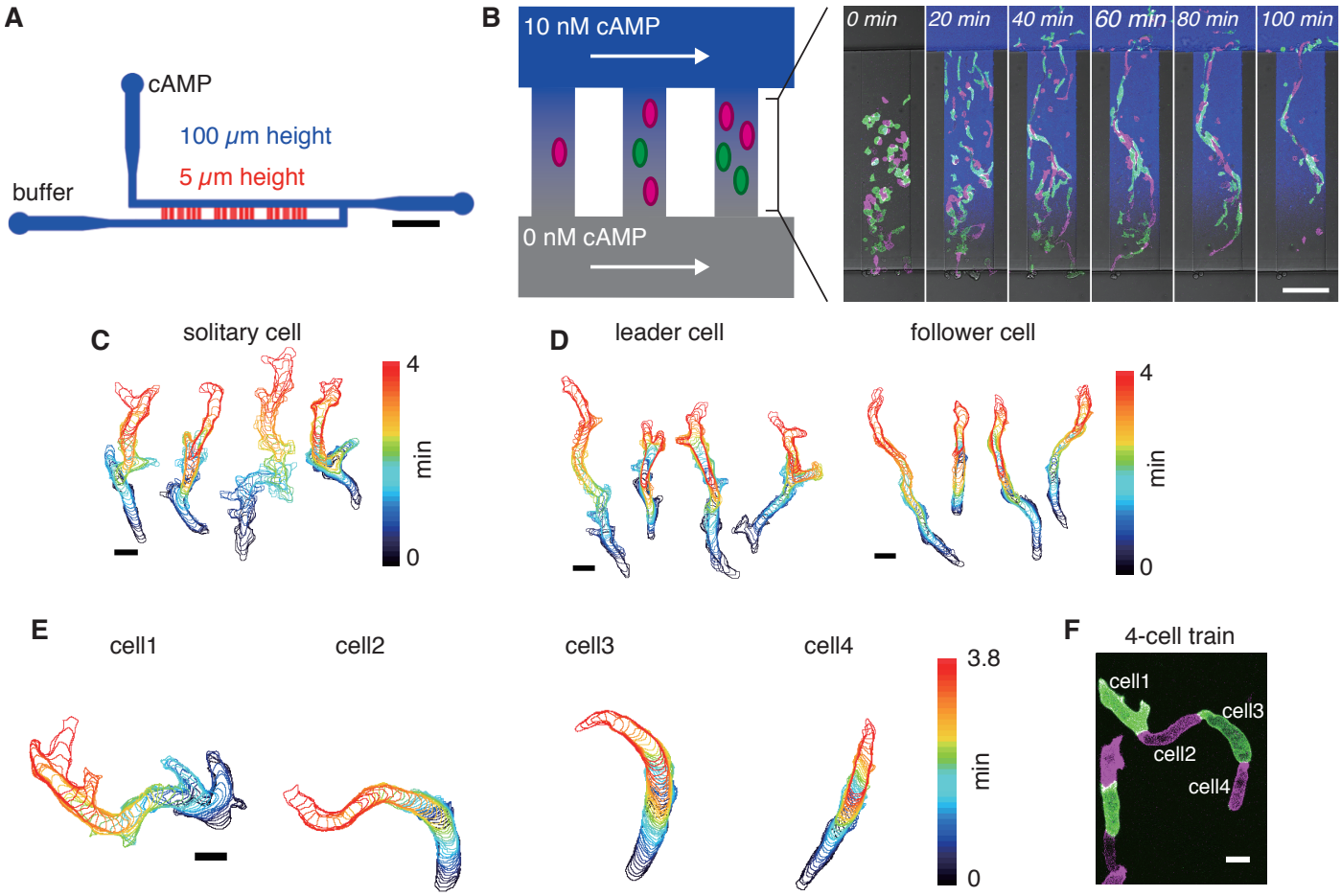

Fig. S3. Microfluidics-based assays of train migration.

(**A** and **B**) An overview of the gradient chamber (A**,** scale bar, 2 mm) and a blowup (B, Scale bar, 100 μm). Open spaces between a microfabricated piece of PDMS and a bonded glass coverslip formed channels. A linear concentration gradient of cAMP was formed by passive diffusion in a narrow low-ceiling channels (red; 100 μm width and 5 μm height, 500 μm length) that bridge two large channels (blue; height 100 μm) that serves as a source and a sink. PB with or without cAMP (final concentration 10 nM) was perfused at 8-10 μL/min using a MFCS from the lower and upper inlet, respectively. 50 μM SQ22536 was included in the buffer to inhibit adenylyl cyclase. Confocal timelapse sequence of cells (GFP-Lifeact (green) and Lifeact-RFP (magenta) expressing cells for identification) forming trains as they migrate toward high cAMP concentrations (B, right panel). 5 μg/ml Atto425 was included in the cAMP solution as an indicator of the gradient profile (blue). (**C** to **E**) Cell morphologies of migrating cells (streaming-stage) analyzed in a mixed population of GFP-Lifeact and Lifeact-RFP expressing cells (solitary migrating cell (C), leader (middle) and follower cell of 2-cell train (D) and 4-cell train (E). Scale bars, 10 μm. Colors indicate elapsed time. (**F**) The original confocal image for analysis of cell morphologies in (E). See Fig. 2B for the confocal microscopy images for (C) and (D).

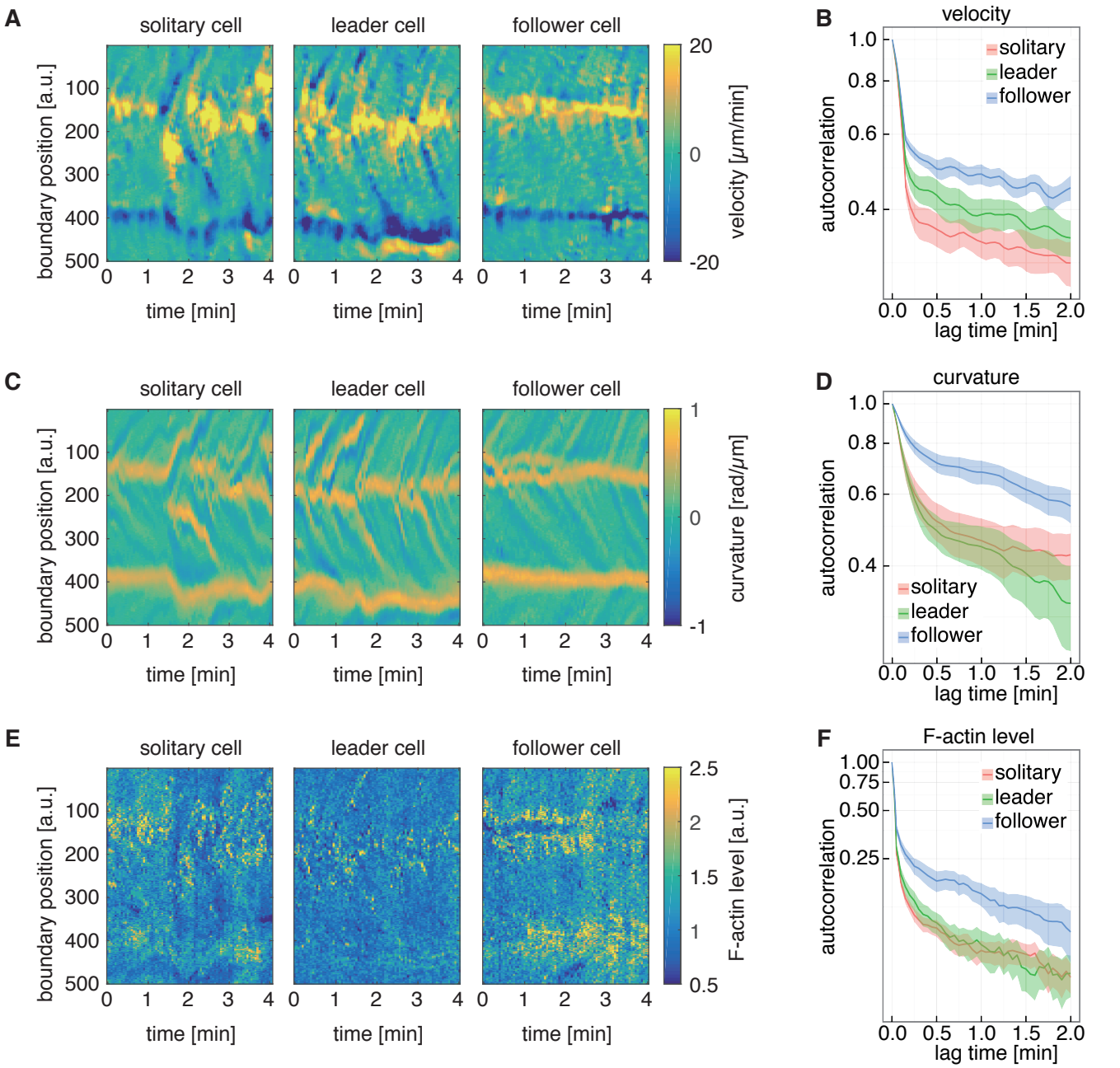

Fig. S4. Quantitative analysis of train cell morphologies.

(**A**, **C**, and **E**) Spatio-temporal change in the velocity (A), curvature (C) and F-actin levels (GFP-Lifeact or Lifeact-RFP fluorescence intensity) (E). 500 positions at cell edge were indexed and their spatial displacements were tracked in time (see *SI Appendix, Materials and methods*). Representative data are shown. (**B**, **D**, and **F**) Autocorrelation of velocity (B), curvature (D), and F-actin (Lifeact) level (F) as a function of time difference. In all cases, follower cells exhibit slower decay indicating their persistence in morphological features. Mean ± s.e.m., solitary: n = 23 cells, leader: n = 19 cells, follower: n = 19 cells.

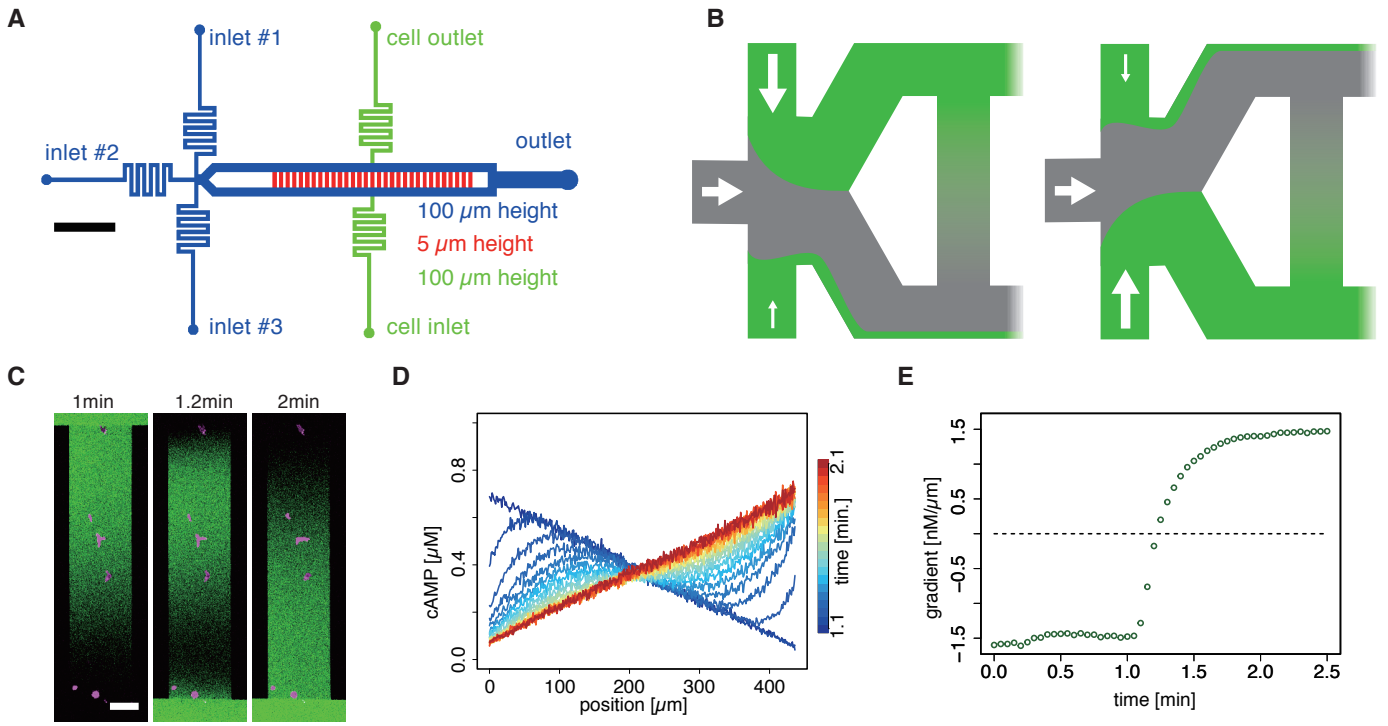

Fig. S5. A microfluidics chamber for gradient reversal.

(**A**) An overview of the gradient chamber. Scale bar, 2 mm. The narrow channels that bridge large source and sink channels follow the basic design of gradient generator in fig S2A. Inlets #1-#3 were connected to MFCS or syringe pumps for perfusion. PB containing cAMP was infused from inlets #1 and #3. PB without cAMP was applied from inlet #2. (**B**) A schematic representation of the basic gradient operation. The initial gradient was set up by applying fast flow from the inlet #1 and #2 (flow rate 5-6 μL/min) compared to that from the inlet #3 (flow rate 0-2 μL/min) so as to prevent the laminar flow from inlet #3 to reach the observation channel (left panel). The rate of flow from inlet #1 and #3 were swapped to reverse the gradient profile (right panel). (**C**) Confocal images of the gradient profile (green; fluorescein) and RFP expressing cells (magenta). Scale bar, 50 μm. (**D**) cAMP concentration profiles along the channel estimated from the fluorescence intensity of fluorescein. 'position' = 0, 436.25 μm indicate the ends of the observation channels. (**E**) Representative time course of the gradient change. The slope of a gradient was estimated by least squares fitting. The flow rate from inlets #1 and #3 were swapped at t = 1 min. The gradient reversal completes in about 2 minutes.

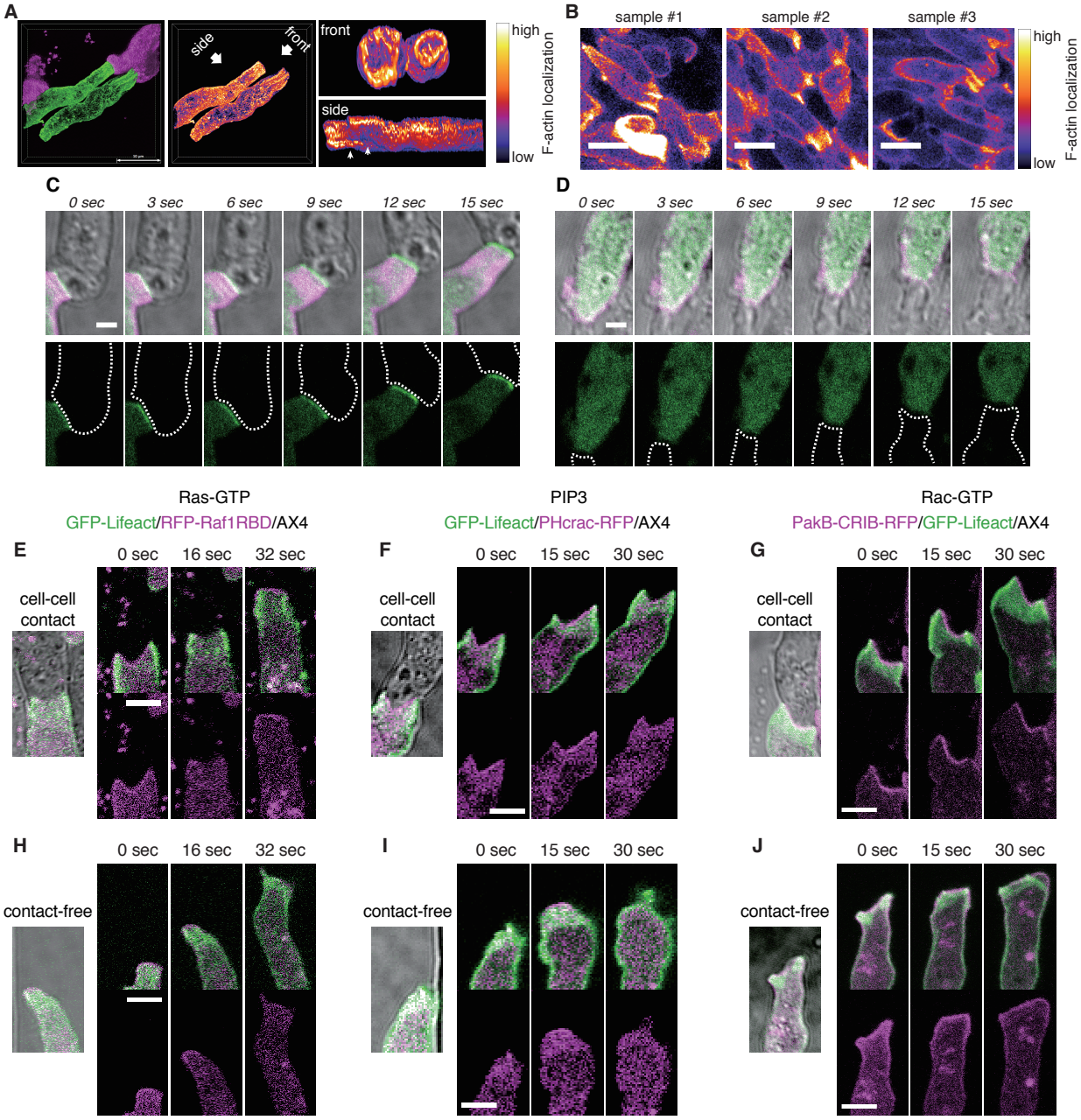

Fig. S6. Distribution of F-actin and leading edge markers.

(**A**) Deconvolved 3D fluorescent profile of GFP-channel (right panels). Leader cells expressing Lifeact-RFP and follower cells expressing GFP-Lifeact migrating in a microchamber. F-actin was most enriched at the ridge of the contact area (front view). Cell-cell contact region detached from substrate. (side view, white arrow). (**B**) Confocal images of Lifeact-RFP fluorescence in cell aggregate (8 hr into starvation, submerged in DB). The distinct F-actin rich front protrusion at the cell-cell contact region was also observed in the cell aggregate. Scale bar, 10 μm. (**C**) A HSPC300-GFP/Lifeact-RFP/AX4 cell following an AX4 cell. (**D**) An AX4 cell following a HSPC300-GFP/Lifeact-RFP/AX4 cell. Green, HSPC300-GFP. Magenta, Lifeact-RFP. Grey; transmitted light. Scale bar, 2 μm. (**E** to **G**) Ras-GTP (E) or PI(3,4,5)P3 (F) or Rac-GTP (G) in follower cells undergoing train migration in a linear cAMP gradient (0-10 nM). Followed cells in contact were non-labeled parental AX4. (**H** to **J**) Contact-free leading edge of cells migrating in a linear cAMP gradient (0-10 nM). Ras-GTP (H), PI(3,4,5)P3 (I) and Rac-GTP (J). Scale Bars, 5 μm. Snapshots were taken from timelapse sequence of GFP-Lifeact/RFP-Raf1RBD/AX4 (E and H), GFP-Lifeact/PHcrac-RFP/AX4 (F and I), PakB-CRIB-RFP/GFP-Lifeact/AX4 (G and I), respectively (magenta; RFP, green; GFP). Note that Ras-GTP and PI(3,4,5)P3 localization were intermittent at both cell-contact-free and cell-contacted leading edge whereas Rac-GTP localization was persistent in both contact-free and cell-contacted leading edge.

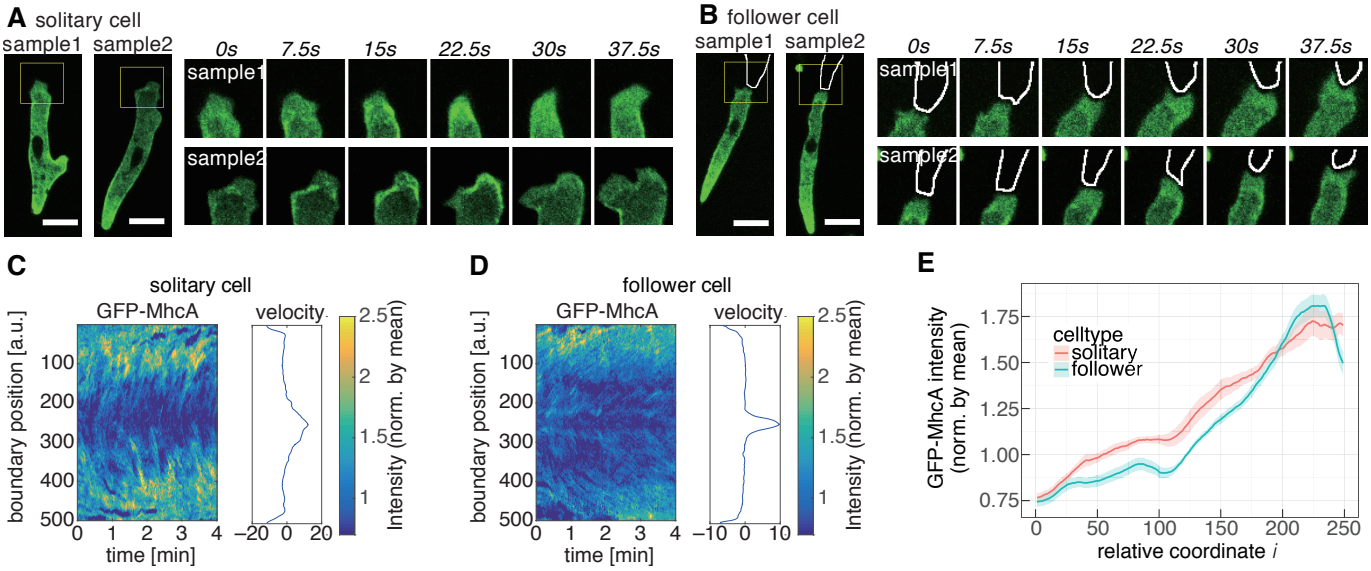

Fig. S7. The anterior Myosin II accumulation is lost by cell-cell contact.

(**A**, **B**) Representative data of GFP-tagged Myosin II heavy chain (GFP-MhcA) expressing cells. A solitary (A) and a follower (B) cell in a microchamber. Time sequences (right panels) are magnified views of yellow rectangular region (left panels). Note the transient Myosin II accumulation at the leading edge of solitary cells (22.5s, A). Scale bars, 10 μm. (**C**, **D**) Spatio-temporal change in the mean GFP-MhcA fluorescent intensity in solitary (C, left panel) or follower (D, left panel) cells. 500 positions at the cell edge were indexed and their spatial displacements were tracked in time (see *SI Appendix, Materials and Methods*). The center position #250 indicates the cell anterior and was defined by the boundary position with the maximum value of average signed velocity. Representative data are shown. (**E**) The mean fluorescence intensity of GFP-MhcA. The average of the left (position #250-*i*; *i* =1 to 249) and right side (position #250+*i*; *i* = 1 to 249). Solitary cell: n=17 cells. Follower cell: n=20 cells. Mean ± s.e.m.

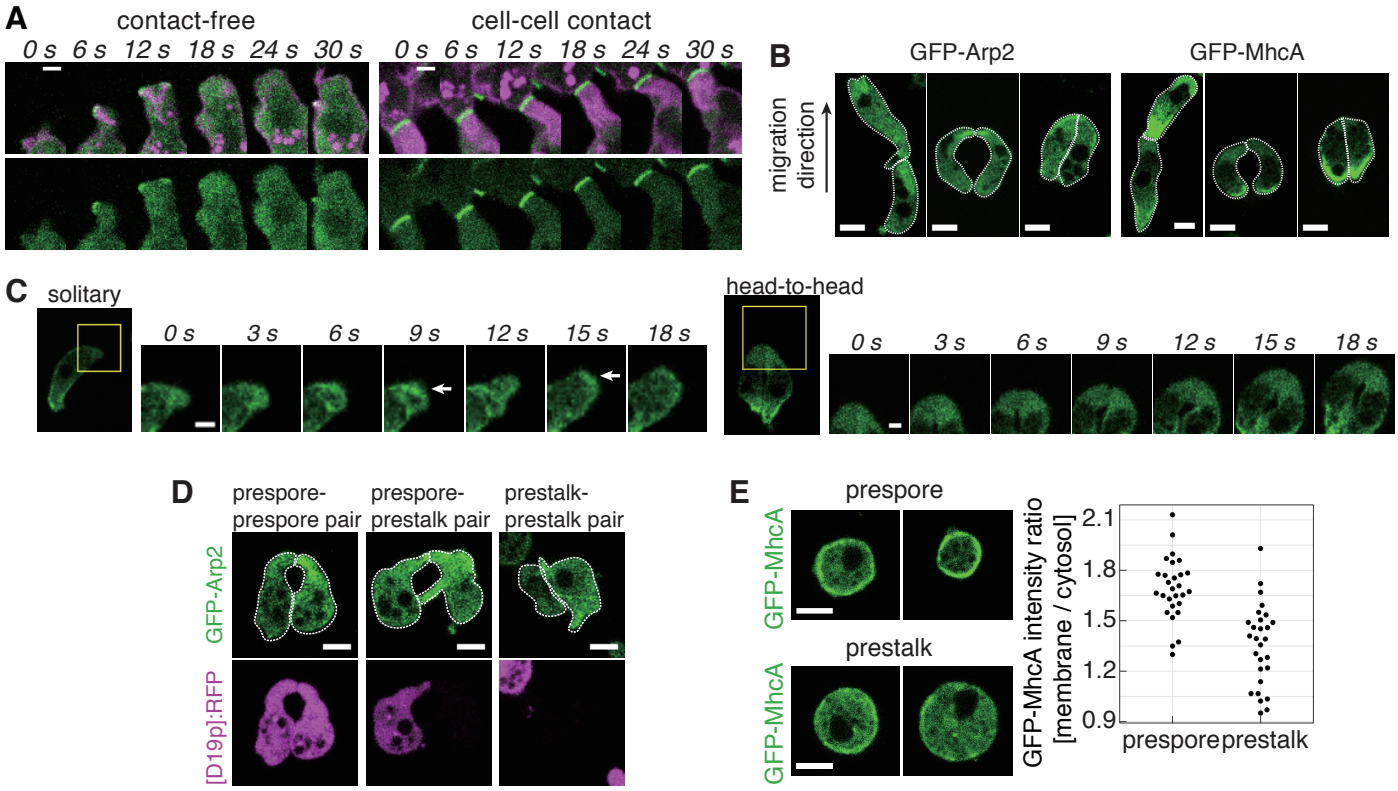

Fig. S8. Contact-dependent protrusion in slug-stage cells.

(**A**) A contact-free (left panels) and a follower cell (right panels) in a micro-chamber (green, HSPC300-GFP; magenta Lifeact-RFP). Scale bars, 2 µm. (**B**) Slug-stage cells expressing GFP-Arp2 (left panels) or GFP-MhcA (Myosin II heavy chain) (right panels) migrating in micro chamber. In addition to head-to-tail contact, head-to-head contact was frequently observed. White dashed lines are marked to indicate the cell contour. All of the cells are prespore. Scale bars, 5 µm. There are two different configurations in head-to-head interaction; cells adhere side by side without gaps (right) or not (middle). Tightly adhered cells tend to migrate faster than the other. (**C**) Time series of GFP-MhcA expressing cells migrating independently (left panels) or in a 2-cell cluster with head-to-head contact (right panels). White arrows indicate transient accumulations of MyosinII at the leading edge. Scale bars, 2 µm. (**D**) Prespore-prespore 2-cell cluster (left panels), prespore-prestalk 2-cell cluster (middle panels) and prestalk-prestalk 2-cell cluster (right panels). Green, GFP-Arp2, magenta, pD19-RFP (prespore marker). White dashed lines are marked to indicate cell contour. Note the symmetric monopodal shape of prespore-prespore cluster cells (left panels). In prespore-prestalk pairs, prespore cells maintain monopodal shape, while prestalk cells exhibited multiple protrusions with high Arp2 accumulation at the contact site (middle panels). In prestalk-prestalk pairs, contact-induced Arp2 accumulation was less marked (right panels). Scale bars, 5 µm. Representative data are shown. (**E**) GFP-MhcA expressing prespore cells (upper left panels) and prestalk cells (lower left panels) treated with 120 µM CK-666 an Arp2/3 inhibitor. Cell type was determined by [D19p]:RFP fluorescence. Under this condition, cells still retain cortical actomyosin. Scale bars, 5 µm. Right panel; the membrane/cytosol intensity ratio of GFP-MhcA (prespore: n = 28 cells, prestalk: n = 28 cells).

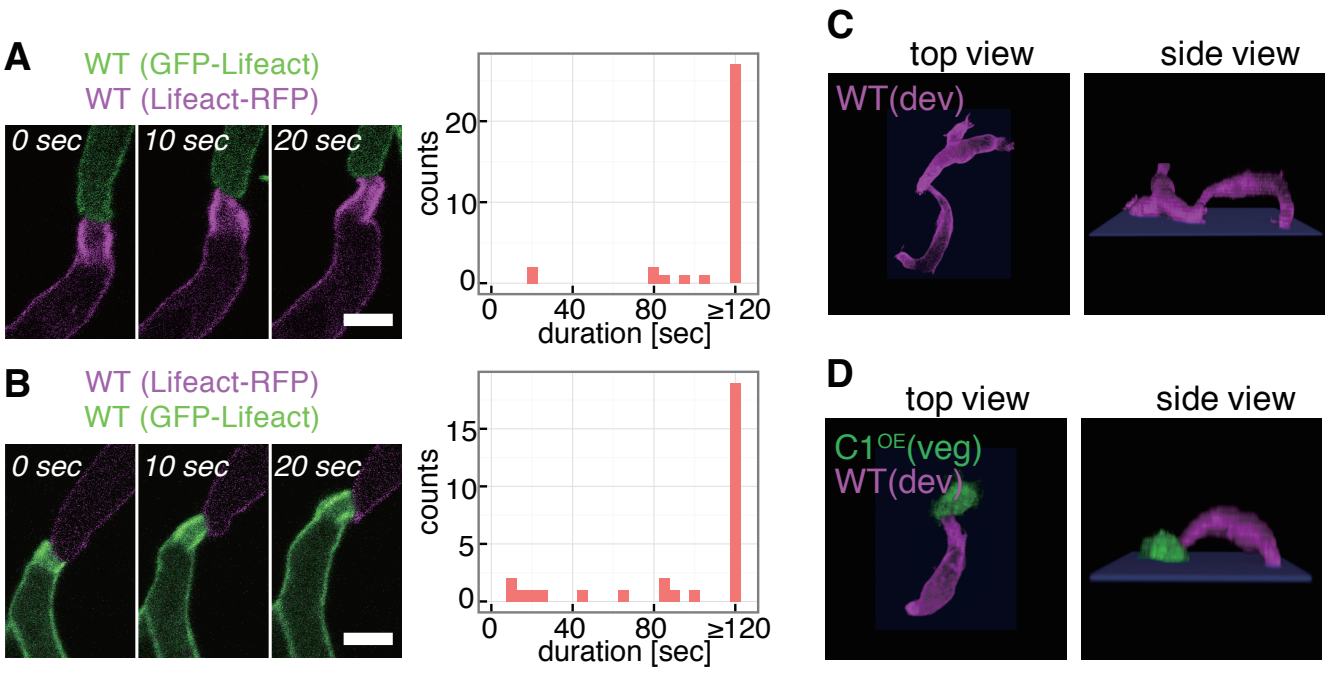

Fig. S9. Contact-dependent protrusion.

(**A** and **B**) A snapshot of GFP-Lifeact expressing cells (green) following RFP-Lifeact expressing cells (magenta) and vice versa (left panels). Duration time of strong F-actin flow at the contact site (A, n = 34 events, B, n = 30 events, right panel). These data serve as controls for Fig. 3A and 3B. (**C** and **D**) Top and side views from 3D confocal images of cell-cell attachment between streaming-stage Lifeact-RFP/AX4 cells (WT(dev)) (C) or between a streaming-stage Lifeact-RFP/AX4 cell (WT(dev)) and a vegetative cell that constitutively expresses TgrC1 ($C1^{OE}$(veg)) (D). Cells were seeded on a glass bottom dish. Without vertical confinement, follower cells detached from the substrate except at the tail. A streaming-stage cell attached to a TgrC1 over-expressing vegetative cell also showing similar detachment from the glass substrate.

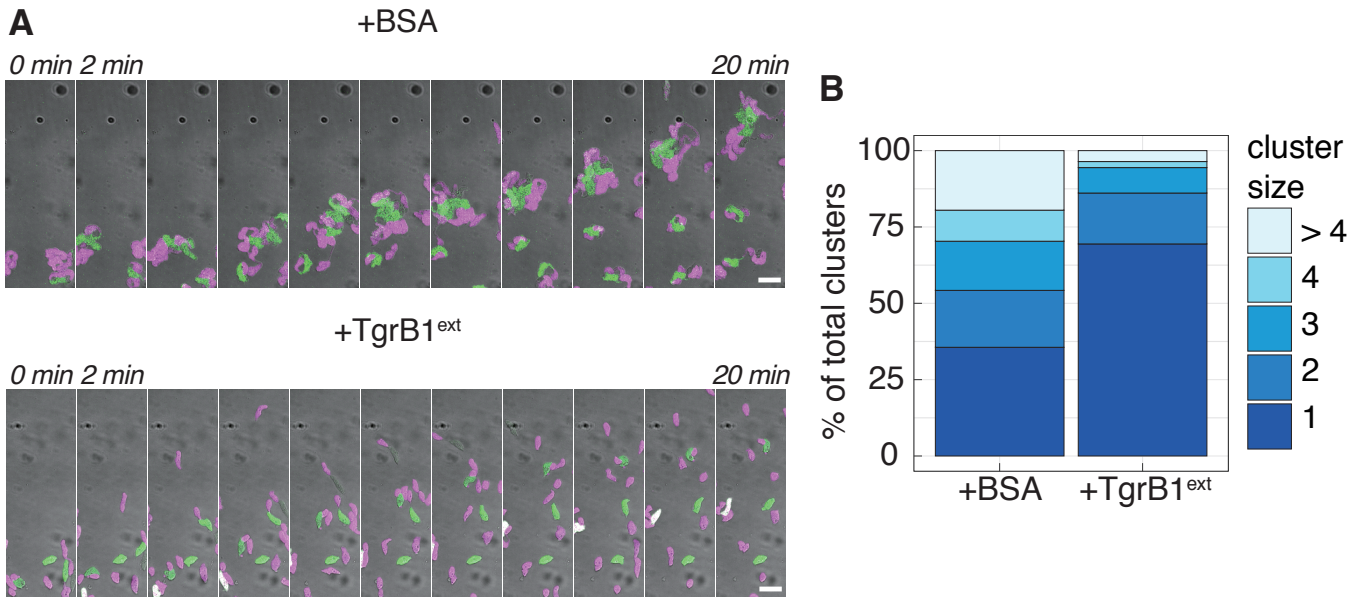

Fig. S10. Migration of slug-stage cells in a cAMP gradient.

(**A**) Timelapse observations of slug-stage cells (magenta, prespore cells; green prestalk cells) in a gradient microchamber (0-1 µM cAMP; bottom to top). Cells remained in clusters under BSA application (mock control; upper panels), whereas cells were dispersed and migrated individually under TgrB1^{ext} application (lower panels). Scale bar, 20 µm. (**B**) Cell cluster size. The number of cells within cell clusters were counted for snapshots taken from four separate gradient channels. Total cell samples: 360 (+BSA), 393 (+TgrB1^{ext}).

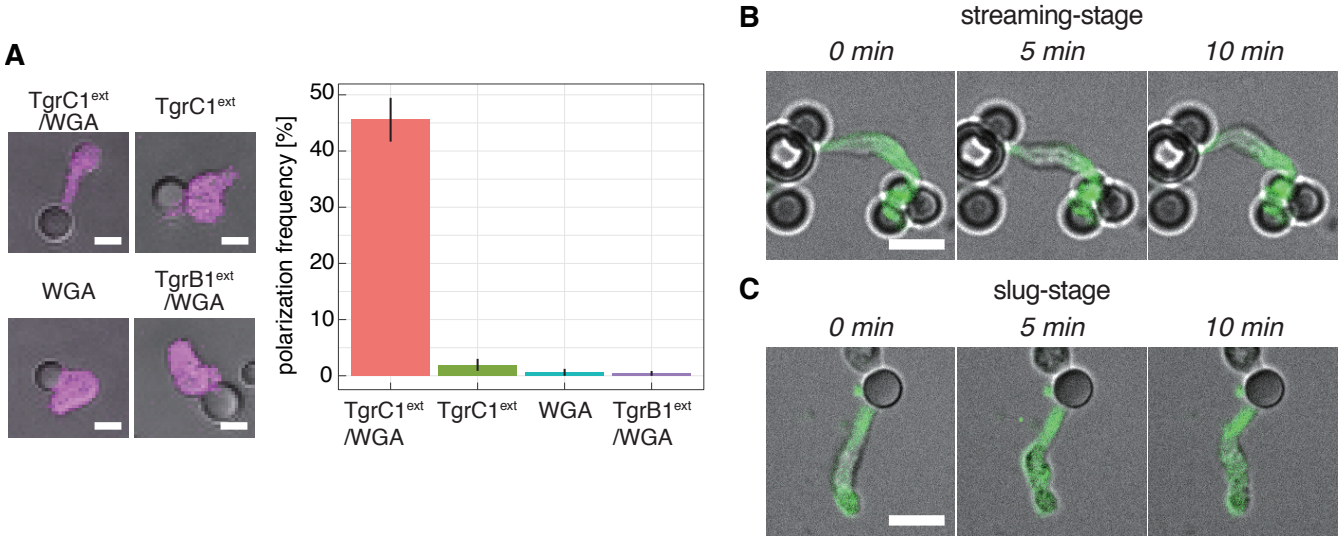

Fig. S11. A contact with a TgrC1^{ext}/WGA coated microsphere induces a protrusion at the contact site.
(**A**) Slug-stage Lifeact-RFP/AX4 cells (magenta) in contact with a microsphere (greyscale; transmitted light) coated with TgrC1^{ext} and WGA (upper left panel), TgrC1^{ext} only (upper middle panel), WGA only (lower left panel) or TgrB1^{ext} and WGA (lower middle panel). Scale bars, 5 µm. Occurrence of protrusions at cell-bead contact sites (right panel; mean ± s.e.m., n = 3 trials; total samples: 335 (TgrC1^{ext}/WGA), 100 (TgrC1^{ext}), 161 (WGA), 441 (TgrB1^{ext}/WGA)). (**B**, **C**) A streaming-stage (6 hr cAMP pulsing, C) and a slug-stage (21 hr after starved on Agar, D) cell (GFP-Lifeact/AX4) attached to TgrC1^{ext}/WGA coated microsphere. Scale bars, 10 µm.

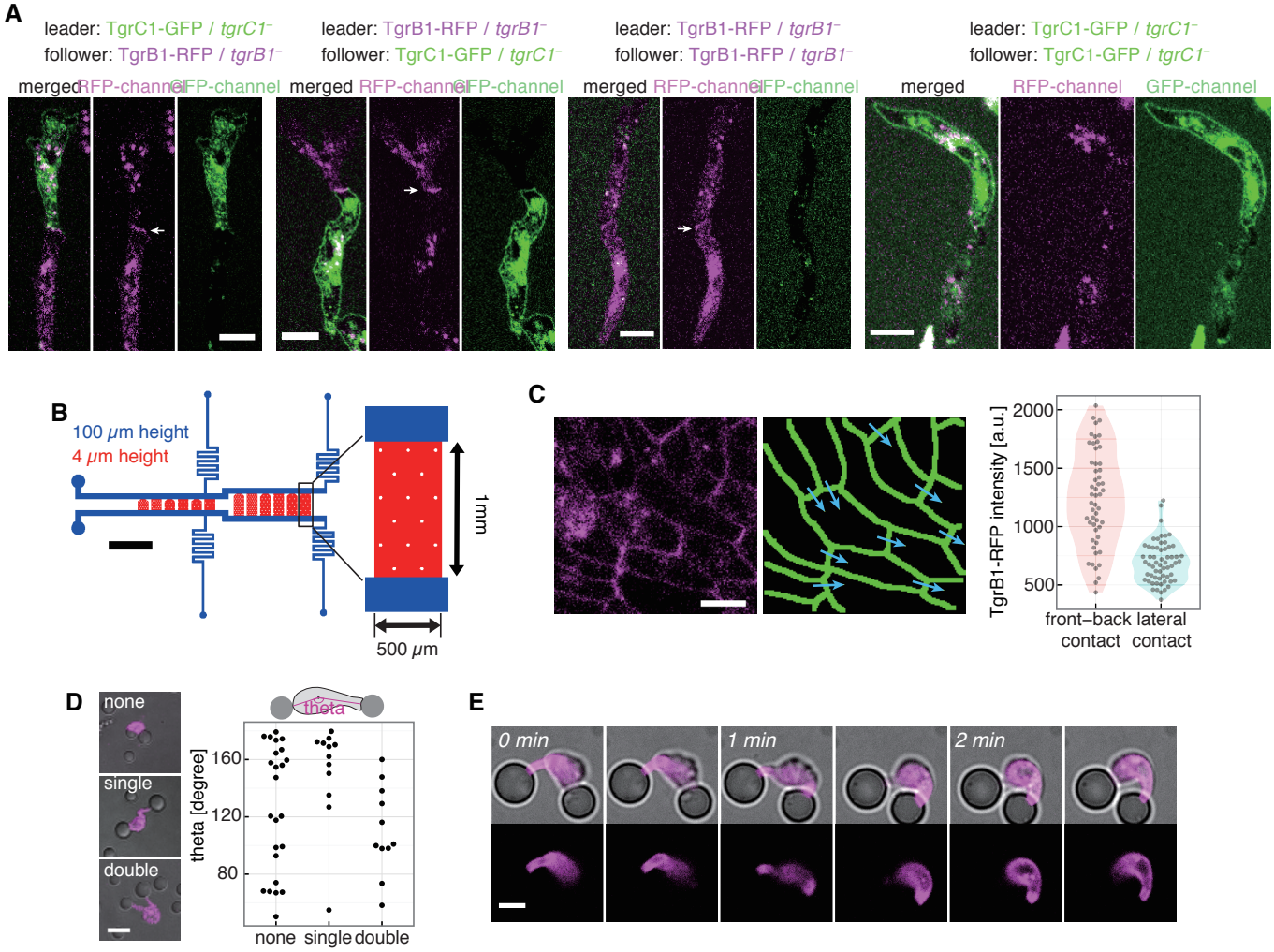

Fig. S12. Distribution of TgrB1 and TgrC1, and cell response to microspheres coated with TgrC1^{ext} and WGA.

(**A**) Train migration of streaming-stage cells in a microfluidic gradient chamber (0-10 nM cAMP). Cells express either TgrC1-GFP or TgrB1-RFP under the native promoter in the respective knockout background. White arrows indicate TgrB1-RFP accumulation at cell-cell contact sites. Note uniform distribution of plasma-membrane bound TgrC1-GFP. (**B**) The low-ceiling chamber for imaging flat aggregates. The low-ceiling channels in the gradient chamber (fig. S4) was expanded in area. Pillars of 20 μm diameter (white circles) were placed at 100-200 μm intervals to support the ceiling. Scale bar, 2 mm. (**C**) Snapshots of TgrB1-RFP expressing streaming-stage cells forming a monolayer aggregate in a microchamber (upper left panel) and manually extracted cell contours (lower left panel; light blue arrows are direction of cell migration). Scale bar, 15 μm. Mean fluorescence intensities of TgrB1-RFP (right panel) at the front-back (n = 53 sites) and the lateral contact site (n = 60 sites). The position of contact sites relative to the direction of cell migration was manually identified. (**D**) Cells attached to two TgrC1^{ext}/WGA coated beads. Slug-stage Lifeact-RFP expressing (from top to bottom; 0, 1, 2 protrusions at cell-bead contact region). Angular distribution of the positions of two attached beads measured from the cell centroid (right panel; no protrusion (n = 24 cells), single protrusion (n = 12 cells), two protrusions (n = 11 cells)). Scale bar, 10 μm. (**E**) A selective protrusion in cells attached to two TgrC1^{ext}/WGA-coated beads. A protrusion formed on a bead disappeared while another protrusion formed on the other bead (t = 1 min). Lifeact-RFP/AX4 (upper panels, merged; lower panels, RFP). Scale bar, 5 μm. All snapshots are from representative data.

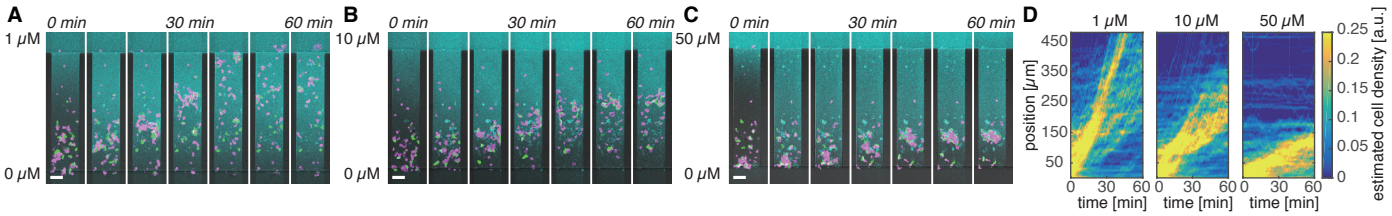

Fig. S13. Concentration dependence of chemotaxis.

(**A** to **C**) Prespore (magenta) and prestalk cells (green) dissociated from slugs in 0-1 μM (A), 0-10 μM (B) and 0-50 μM (C) cAMP gradients. Note that cells move through and exit the channels within 60 minutes in a 0-1 μM gradient, whereas they stop in the middle in 0-10 and 0-50 μM gradients. Scale bars, 50 μm. (**D**) Merged chemotactic trajectories. Cell masks in the GFP- and RFP-channels averaged over 9 lanes and normalized. Cell density 0 and 1 (colormap) correspond to space completely empty or fully occupied by the cells, respectively.

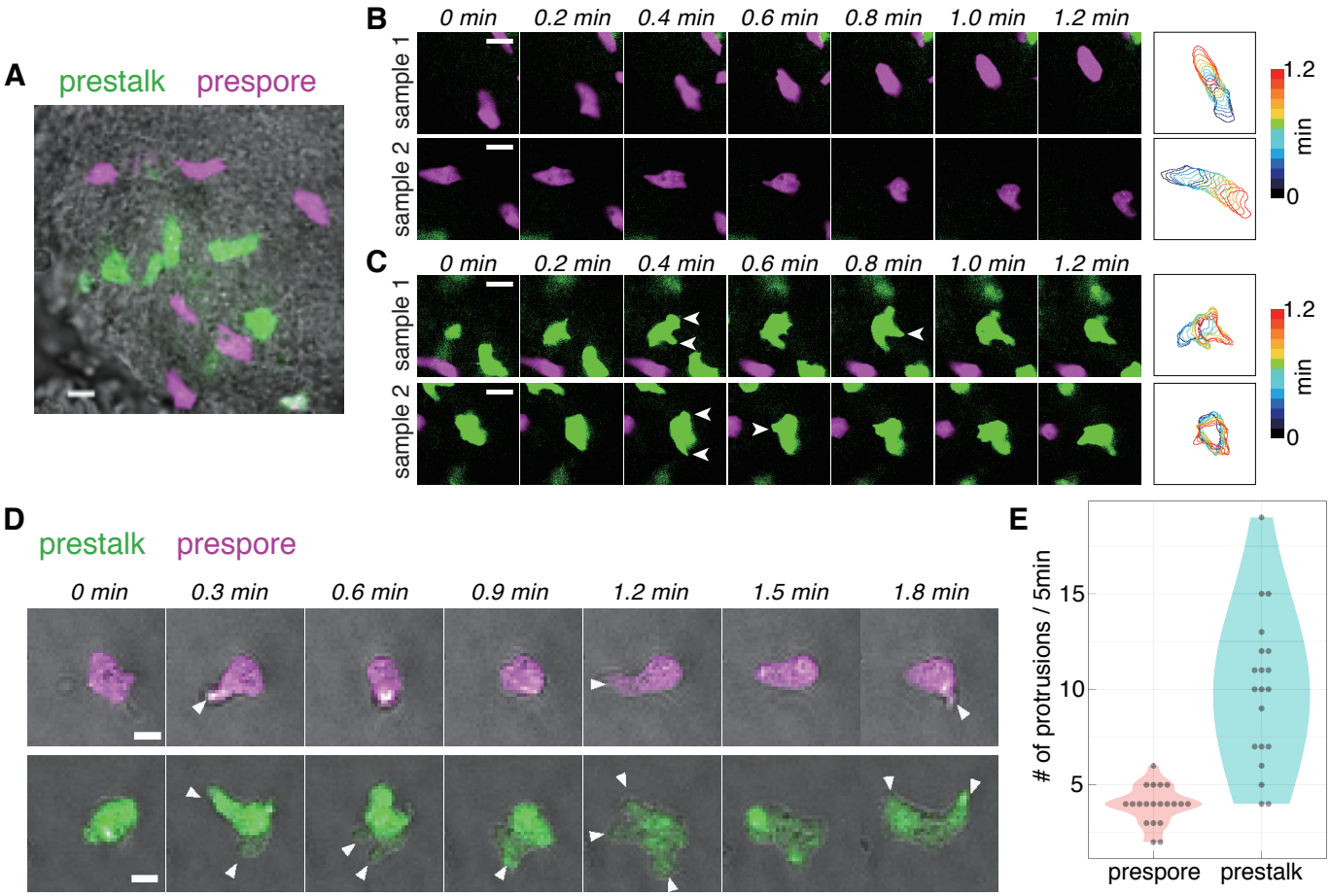

Fig. S14. Polarity dynamics in prestalk and prespore cells.

(**A**) A regenerating mound of AX4 cells (no fluorescence) including a 10% cell-type marker strain pEcmAO-GFP/pD19-RFP/AX4 cells (Green, [ecmAOp]:GFP, prestalk cell marker; Magenta, [D19p]:RFP prespore cell marker). Scale bar, 10 μm. (**B**,**C**) Two representative timeseries of prespore cells (B) and prestalk cells (C) in the regenerating mound (A). Note the monopodal morphology of prespore cells and multiple protrusions in prestalk cells (white arrows). Scale bars, 10 μm. (**D**) Dissociated slug-stage cells (pEcmAO-GFP/pD19-RFP/AX4) on a cover-slip in PB without cell-cell contact. Green, [ecmAOp]:GFP, prestalk cell marker. Magenta, [D19p]:RFP prespore cell marker. White arrowheads are marked to indicate protrusions. Scale bars, 5 μm. (**E**) Number of protrusions within 5 minutes was counted (prespore: n = 20 cells, prestalk: n = 20 cells).

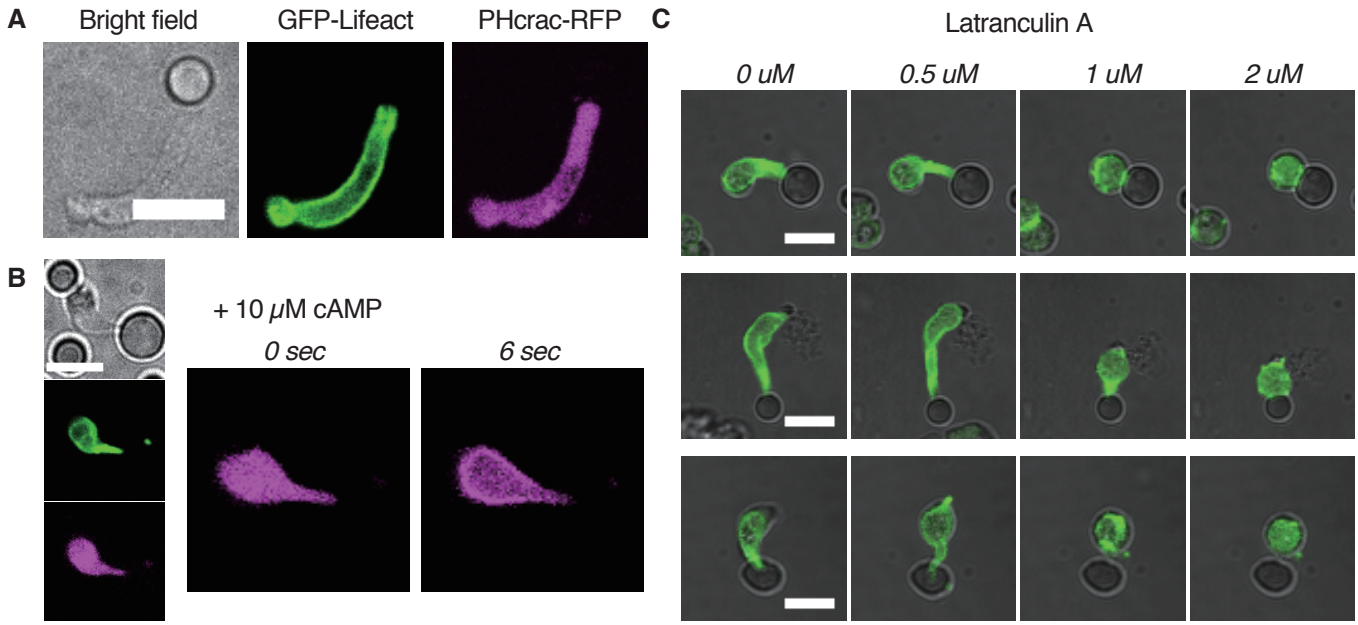

Fig. S15. Cell-contact dependent protrusions are distinct from phagocytic cups.

(**A**) A slug-stage cell (GFP-Lifeact/PHcrac-RFP/AX4) attached to a TgrC1^{ext}/WGA-coated microsphere. Scale bar, 10 µm. Note lack of obvious localization of PHcrac-RFP at the cell-bead interface. (**B**) A slug-stage cell (GFP-Lifeact/PHcrac-RFP/AX4) attached to a TgrC1^{ext}/WGA coated microsphere stimulated with uniform 10 µM cAMP (at time t = 0 sec). Scale bar, 10 µm. cAMP-induced transient translocation of PHcrac-RFP (magenta) to the plasma membrane occurs independently of the Tgr-mediated contact. (**C**) Incremental addition of LatranculinA to slug-stage cells (green; GFP-Lifeact/AX4, Grey; transmitted light) attached to a TgrC1^{ext}/WGA-coated microsphere. Scale bars, 10 µm. Moderate dosages of LatA shortened the protrusion however the contact site remained narrow until cells became completely round at high dosages.

Supplementary Movie Legends

Movie S1. Two modes of collective cell migration - contact-mediated and chemotaxis-mediated - revealed by administration of exogenous TgrB1^{ext} and PDE.

Time-lapse movies of regenerating mounds under +BSA (mock control), +TgrB1^{ext}, +PDE, +TgrB1^{ext}/+PDE or +TgrC1^{ext} treatment. Prespore (magenta) and prestalk (green) cells.

Movie S2. High magnification movies of regenerating mound.

Time-lapse movies of regenerating mounds (green, GFP-Lifeact) under BSA (mock control), TgrB1^{ext}, TgrC1^{ext} and PDE application 2 hr after plating.

Movie S3. Train migration of *Dictyostelium* cells.

A time-lapse movie of streaming-stage (6 hr cAMP pulsed) Lifeact-RFP/AX4 (magenta) and GFP-Lifeact/AX4 (green) cells in a linear cAMP gradient (0 to 10 nM. Blue, ATTO425).

Movie S4. Turning response to a gradient reversal.

Time-lapse movies of streaming-stage Lifeact-RFP/AX4 (magenta) cells responding to a reversal of cAMP gradient (green; fluorescein). A solitary cell (left) and a 2-cell train (right).

Movie S5. F-actin dynamics at the leading edge of migrating cells.

Time-lapse movies of streaming-stage cells expressing HSPC300-GFP (green) and Lifeact-RFP (magenta) in a linear cAMP gradient (0 to 1 μM). A solitary cell (left) and a follower cell (right).

Movie S6. Contact-mediated forward propulsion revealed by immobilization of a leader cell.

Time lapse movies of 2-cell trains in a microfluidic gradient chamber. The follower (left) or the leader cell (right) was irradiated at t = 0 sec by UV light.

Movie S7. Growth-stage cells over-expressing TgrC1 are able to lead a cell train.

Time-lapse movies of a streaming-stage Lifeact-RFP/AX4 (magenta) cell following a TgrC1-GFP over-expressing vegetative cell (low fluorescence) in a folate gradient.

Movie S8. Slug-stage cells in a cAMP gradient and the effect of TgrB1^{ext} application.

Time-lapse movies of slug-stage cells (green, prestalk; magenta, prespore) in a linear cAMP gradient (0 to 1 μM). 1 mg/mL BSA (left) or TgrB1^{ext} (right) were included in the perfused buffer and cAMP solution.

Movie S9. TgrC1^{ext}/WGA coated-microsphere induces a leading edge that persists at the contact site.

Time-lapse movies of a slug-stage cell expressing HSPC300-GFP (green) and Lifeact-RFP (magenta) with or without attachment to a TgrC1^{ext}/WGA coated microsphere.

Movie S10. TgrB1 localization is selective to single front-back contacts.

A time-lapse movie of a chimeric monolayer formed by streaming-stage TgrB1-RFP/*tgrB1*$^{-}$ (magenta) cells and GFP-Lifeact/AX4 cells (green) in a microchamber. The cell #1 (magenta) was first following cell #2 then switched to cell #3; TgrB1 at the leading edge of cell #1 (magenta) first accumulated at the interface with cell #2 then switched to cell #3 (green).

Movie S11. Prespore and prestalk cells attached to a TgrC1^{ext}/WGA-coated microsphere.

Time-lapse movies of slug-stage cells attached and polarized to a TgrC1^{ext}/WGA-coated microsphere. Prespore (left panels) and prestalk (right panels) cells.

Movie S12. Prespore and prestalk cells attached to TgrC1^{ext}/WGA-coated microsphere stimulated with a cAMP gradient.

Time-lapse movies of slug-stage cells attached to TgrC1^{ext}/WGA-coated microspheres and stimulated with a cAMP gradient (green) formed by a cAMP-filled glass needle. Prespore cells remained polarized and attached to coated-beads (left panels). Prestalk cells detached from the bead and migrated towards the cAMP source (right panels).

Supplementary References

1. Chen G, Xu X, Wu X, Thomson A, Siu C-H (2014) Assembly of the TgrB1-TgrC1 cell adhesion complex during Dictyostelium discoideum development. *Biochem J* 459(2):241–249.

2. Nellen W, Silan C, Firtel RA (1984) DNA-mediated transformation in Dictyostelium discoideum: regulated expression of an actin gene fusion. *Mol Cell Biol* 4(12):2890–2898.

3. Lemieux MG, et al. (2014) Visualization of the actin cytoskeleton: different F-actin-binding probes tell different stories. *Cytoskeleton (Hoboken)* 71(3):157–169.

4. Fukujin F, Nakajima A, Shimada N, Sawai S (2016) Self-organization of chemoattractant waves in Dictyostelium depends on F-actin and cell-substrate adhesion. *J R Soc Interface* 13(119):20160233.

5. Asano Y, et al. (2004) Keratocyte-like locomotion in amiB-null Dictyostelium cells. 59(1):17–27.

6. Moores SL, Sabry JH, Spudich JA (1996) Myosin dynamics in live Dictyostelium cells. *Proc Natl Acad Sci USA* 93(1):443–446.

7. Veltman DM, King JS, Machesky LM, Insall RH (2012) SCAR knockouts in Dictyostelium: WASP assumes SCAR's position and upstream regulators in pseudopods. *J Cell Biol* 198(4):501–508.

8. Nakajima A, Ishihara S, Imoto D, Sawai S (2014) Rectified directional sensing in long-range cell migration. *Nat Commun* 5:5367.

9. Nikolaev VO, Bünemann M, Hein L, Hannawacker A, Lohse MJ (2004) Novel single chain cAMP sensors for receptor-induced signal propagation. *J Biol Chem* 279(36):37215–37218.

10. Sawai S, Thomason PA, Cox EC (2005) An autoregulatory circuit for long-range self-organization in Dictyostelium cell populations. *Nature* 433(7023):323–326.

11. Gregor T, Fujimoto K, Masaki N, Sawai S (2010) The onset of collective behavior in social amoebae. *Science* 328(5981):1021–1025.

12. Nakajima A, Ishida M, Fujimori T, Wakamoto Y, Sawai S (2016) The microfluidic lighthouse: an omnidirectional gradient generator. *Lab Chip* 16(22):4382–4394.

13. Nakajima A, Sawai S (2016) Dissecting Spatial and Temporal Sensing in Dictyostelium Chemotaxis Using a Wave Gradient Generator. *Methods Mol Biol* 1407(Chapter 8):107–122.

14. Alvarez-Curto E, Weening KE, Schaap P (2007) Pharmacological profiling of the Dictyostelium adenylate cyclases ACA, ACB and ACG. *Biochem J* 401(1):309–316.

15. Xu X, Meier-Schellersheim M, Yan J, Jin T (2007) Locally controlled inhibitory mechanisms are involved in eukaryotic GPCR-mediated chemosensing. *J Cell Biol* 178(1):141–153.